Polymer Diffusion in Semicrystalline Polymers. 2. Atactic Polystyrene-*d* Transport into Atactic and Isotactic Polystyrene

John G. Van Alsten,* Steven R. Lustig, and Benjamin Hsiao

Central Research Division, E. I. du Pont de Nemours & Co., Inc., Experimental Station, Route 141, Wilmington, Delaware 19880-0356

Received September 21, 1994; Revised Manuscript Received February 17, 1995[⊗]

ABSTRACT: The transport of monodisperse, atactic polystyrene-*d* (aPS-D) into atactic polystyrene (aPS) melts and isotactic polystyrene (iPS) semicrystalline matrices has been characterized by a quantitative ATR-FTIR technique. Values of aPS-D tracer diffusion coefficients in aPS melts compare very well with previous literature indicating the effects of (i) diffusant molecular weight holding constant the matrix molecular weight and (ii) matrix molecular weight holding constant the diffusant molecular weight. Semicrystalline morphologies of iPS were characterized extensively by DSC, microscopy, and SAXS as a function of temperature. Non-Fickian transport kinetics are observed during the imbibition of aPS-D into semicrystalline iPS at low temperatures and high penetrant molecular weights. There are two apparent time regimes of non-Fickian kinetics. The first regime of imbibition kinetics occurs at early times, where the uptake can be described by Fickian mutual diffusion kinetics. Later, there is a decrease in the imbibition rate and the rates of continued imbibition are no longer Fickian. The transition to a slower transport kinetics regime can be identified with a time scale over which penetrant macromolecules in amorphous pockets explore the bottlenecks between crystalline, dendritic obstacles.

Introduction

Very little fundamental understanding exists concerning macromolecular transport into semicrystalline, polymeric materials. These interpenetration kinetics have important ramifications in a variety of high-performance engineering applications which apply crack healing, fusion bonding, welding, and the diminution of molding lines. In addition, these kinetics provide very interesting information concerning non-Fickian macromolecular transport phenomena and the dynamics of macromolecules ensconced within a complex morphology. Transport might be expected to depend on factors such as the degree of crystallinity, interlamellar morphology, penetrant size, and penetrant–matrix interactions. We begin to explore these phenomena experimentally by characterizing the imbibition of monodisperse PS-D into both precrystallized and amorphous PS matrices.

In our previous work[1] we investigated the interdiffusion and bonding between an amorphous resin, poly(ether imide) (PEI), and a typical family of high-performance thermoplastic copolymers, poly(aryl ether ketone ketone) (PEKK). PEI and PEKK form a single, thermodynamically miscible phase in the melt state. Mutual interdiffusion between melts was found to be described well by Fickian kinetics. In contrast, PEI transport into a semicrystalline PEKK matrix occurs with non-Fickian overall kinetics. Two distinct time scales of sorption kinetics are observed during PEI sorption in PEKK with a stable, semicrystalline morphology. The early time transport can be described by Fickian mutual diffusion kinetics although the amount of PEI imbibition remains far below that expected for saturation in the PEKK amorphous pockets. Later, there is a transition in the sorption kinetics which then proceed much slower than a Fickian rate. We surmised that the transition to a slower transport kinetics regime can be identified with a time scale over which penetrant macromolecules in amorphous pockets explore the bottlenecks between crystalline, dendritic obstacles.

[⊗] Abstract published in *Advance ACS Abstracts,* April 1, 1995.

Table 1. Structure, Degree of Polymerization (N) and Polydispersity (M_w/M_n) for the Polystyrenes Used in This Study

structure	N	M_w/M_n
penetrants and matrices		
perdeuterated, atactic	45	1.04
	105	1.02
	275	1.06
	720	1.03
	1 040	1.02
	5 000	1.07
matrices		
hydrogenated, atactic	660	1.03
	1 040	1.05
	19 170	1.06
hydrogenated, isotactic	5 400	1.26

In this work, we extend our investigation to model polystyrene penetrant–matrix systems. Semicrystalline isotactic polystyrene (iPS) matrices are each fully annealed to stable, impinging spherulitic morphologies. The atactic, perdeuterated polystyrene (aPS-D) penetrants are monodisperse and uncrystallizable. This will permit the characterization of molecular size effects while minimizing possible artifacts due to the distribution of chain lengths. We apply a quantitative, infrared technique[2] recently developed in our laboratory to characterize the transport kinetics between the penetrant–matrix system and provide new SAXS, WAXS, DSC, and morphological characterizations of the matrices before and after the penetrant imbibition. For consistent comparisons, we also characterize the transport of these perdeuterated penetrants into melts of high molecular weight atactic polystyrene (aPS).

Experimental Section

Materials and Preparation. Table 1 summarizes the molecular characteristics of the polystyrene penetrants and matrices used in this investigation. Perdeuterated, atactic polystyrenes (Polymer Laboratories) were prepared anionically and have very narrow molecular weight distributions. Thin films of these materials were prepared by spin coating xylene solutions directly onto silicon ATR crystals followed by annealing at 150 °C in a nitrogen-purged vacuum oven. The thicknesses of these films, typically 500–1000 Å, were then determined by spectroscopic ellipsometry (Sopra). Isotactic

0024-9297/95/2228-3672$09.00/0

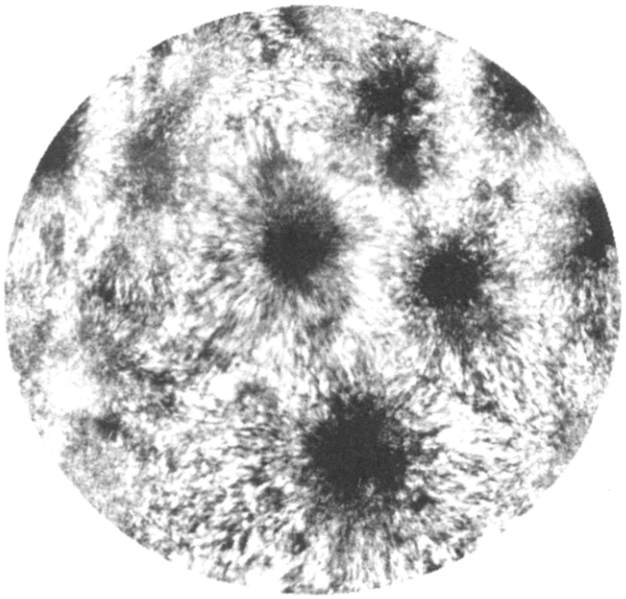

Figure 1. Photomicrograph of a typical isotactic polystyrene matrix utilized in these experiments. The spherulite diameters are ca. 60 μm. The sample is between two crossed polarized light filters.

polystyrene of $N_p = 5400$ (Pressure Chemical) was obtained in powder form. NMR analysis by the manufacturer indicated stereochemical homogeneity greater than 99% isotactic triads. This material was formed into ca. 100 μm thick matrix films by sandwiching the powder between Kapton films, melt pressing at 300 °C, and rapidly quenching to room temperature. The matrices were then crystallized at 180 °C for 4 h between the platens of a preheated press under a 50 psi load. Such treatment was sufficient to produce films whose volume was filled with impinging spherulites as determined by polarized light microscopy (see Figure 1). Surface profilimetry (Sloan Dektak II) indicated that the surface roughness of these films was approximately 35 Å as measured by the 12.5 μm radius of the probing tip.

Diffusion Measurements. The sorption kinetics of atactic, perdeuterated polystyrene penetrants into amorphous (atactic) and semicrystalline (isotactic) matrices of polystyrene were characterized using the attenuated total reflectance infrared (ATR-IR) technique which we have described in previous publications.[1,2] Briefly, this technique measures the loss of a polymer from its coating on the face of an infrared ATR element into a second, infrared-distinguishable polymer matrix in contact with the penetrant film. As the coating polymer migrates away from the surface of the ATR element, it becomes undetectable by the evanescent ATR-IR beam. A penetrant's time-dependent, infrared spectral absorbance is normalized between the initial and equilibrium values to provide a normalized mass uptake curve as a function of time. This curve can be predicted mathematically at any time by convoluting the spatial dependences of the polymer's concentration history with the detecting electric field of the ATR-IR beam. We have shown that these uptake measurements yield excellent descriptions of simple Fickian diffusion, but the technique is of course general to any situation in which the concentration profile can be represented mathematically.

To begin an experiment, the diffusion couple is produced by placing the matrix film in contact with the ATR crystal coated with the penetrant thin film. A sheet of silicone rubber was used on the back of the thicker matrix film to ensure uniform mechanical contact in the polymer bilayer. This assembly was then mounted in a stainless steel cell which is equipped with resistive heating elements and a temperature controller. Once the assembly is aligned within an FTIR spectrometer, experiments commence by rapidly heating the cell from room temperature to the experimental temperature. The heating time was approximately 20 s for the largest interval between the glass transition temperature of the materials and the experimental temperature. Unless otherwise stated, experiments were performed at 170 °C. This temperature is 10 deg below the annealing temperature of the semicrystalline matrix, hence minimizing the contribution of gross morphological changes to the transport behavior.

Table 2. Tracer Diffusion Coefficients (D) for a aPS-D Penetrants in aPS Matrices Depending on Temperature, Penetrant Degree of Polymerization ($N_{penetrant}$), and Matrix Degree of Polymerization (N_{matrix})

temp (°C)	$N_{penetrant}$	N_{matrix}	D (cm^2/s)
130	45	19 170	2.2×10^{-12}
	1 040	19 710	2.6×10^{-16}
150	45	19 710	1.8×10^{-11}
	1 040	19 710	1.0×10^{-14}
170	45	19 710	3.2×10^{-11}
	270	19 710	8.7×10^{-13}
	1 040	19 710	2.0×10^{-13}
	5 000	19 710	2.7×10^{-15}
	1 040	275	3.4×10^{-12}
	1 040	660	1.5×10^{-12}
	1 040	1 560	2.2×10^{-13}

For Fickian mutual diffusion between two miscible, initially stratified layers, the ATR-IR absorbance measure of penetrant uptake, A_t, as a function of time, t, is described in eq 1.[2]

$$\frac{A_t - A_0}{A_\infty - A_0} = 1 - \frac{2\sum_{n=1}^{\infty} \frac{\sin\left(n\pi\frac{b}{a}\right)}{n\pi} \exp\left(-n^2\pi^2\frac{Dt}{a^2}\right)\left[\frac{1+(-1)^{n+1}\exp\left(\frac{-2a}{\lambda}\right)}{1+\left(\frac{n\pi\lambda}{2a}\right)^2}\right]}{\left[1-\exp\left(\frac{-2b}{\lambda}\right)\right] - \frac{b}{a}\left[1-\exp\left(\frac{-2a}{\lambda}\right)\right]} \quad (1)$$

where A_0 and A_∞ are the initial and long-time infrared absorbances, a is the total thickness of the diffusion couple on the ATR element, b is the initial thickness of the penetrant coating, λ is the infrared evanescent penetration depth,[3] and D is the constant mutual diffusion coefficient. The diffusion experiments were typically performed using silicon ATR elements which had been cut to provide a 30° reflection angle. The refractive index of polystyrene, 1.39, was determined from a reflectivity experiment[2] at the C−D stretching frequency of 2150 cm^{-1} and the silicon refractive index, 3.54,[4] is known. Hence the infrared penetration depth is 0.67 μm. Since our experimental values of b are much less than the value of λ, fits to eq 1 yield values of tracer diffusion coefficients.[2] These results are summarized in Table 2.

Characterization of Morphology. The semicrystalline polymer matrix films were characterized using differential scanning calorimetry, polarized light microscopy, wide-angle X-ray scattering (WAXS), and small-angle X-ray scattering (SAXS). Calorigrams were obtained on a DuPont Instruments 9900 using a heating rate of 10 °C/min. Visual observations of melting behavior were performed using a Mettler hot stage mounted on a polarizing microscope where images were recorded by a television camera and video cassette recorder. The microscope was also equipped with a photodiode to measure transmitted light intensity. The weight fraction degree of crystallinity for a representative sample was also estimated from WAXS by deconvolution. Data were collected by a Philips diffractometer (Cu Kα radiation) in a fixed time mode with a step size of 0.05° 2θ and run from 4 to 65° 2θ. SAXS of the annealed samples was carried out with Kratky optics using a scintillation counter and Cu Kα radiation. The data were collected in a step size of 0.01° 2θ, run from 0.12 to 1.4° 2θ, and desmeared High-temperature SAXS measurements were performed at the X3A2 SUNY beamline, National Synchrotron Light Source, Brookhaven National Laboratory ($\lambda_0 = 0.154$ nm). These data were collected using modified

Kratky optics[5] which requires no desmearing treatment and uses a linear position-sensitive detector (Braun). All signals were corrected for sample absorption, background, incident beam fluctuation, and collection time (60 s for each scan) and then smoothed by a low-frequency band-pass filtering routine to enhance the signal to noise ratio.[6]

In order to infer lamellar variables, the SAXS scattering data $I(\theta)$ were corrected for thermal density fluctuations, I_b, using Porod's law. The correlation function $\gamma(r)$ was calculated as

$$\gamma(r) = \frac{1}{2\pi^2}\int_0^\infty (I(q) - I_b)q^2 \cos(qr)\, dq \qquad (2)$$

where $q = 4\pi \sin(\theta)/\lambda_0$ and the scattering spectrum intensity, $I(q)$, was extrapolated to the limits of zero and infinity. A number of quantities can be estimated from $\gamma(r)$ which characterize morphology when one assumes a particular scattering model. We have applied the analysis of Santa Cruz *et al.*[7] as described in our previous work.[1] The long period, L, is determined as the position of the first maximum in $\gamma(r)$. The linear degree of crystallinity x_{CL} is determined from the first intercept of the $\gamma(r) = 0$ line. The lamellar thickness, l_C, is the product of L and x_{CL}, and the invariant Q is the value of $\gamma(0)$. This model is described in more detail in the Results section.

Results

Isotactic PS Morphology. It is desirable to know the extent and distribution of crystalline and motionally restricted amorphous regions, since these act as impediments to the flux of material. Several investigators have previously used electron microscopy to characterize crystalline morphology in melt-quenched iPS. For example, Bassett and co-workers[8-10] concluded that spherulites exhibit a very heterogeneous distribution of crystalline lamellae. At the spherulite nucleus there exists a very dense core of lamellar bundles. As these primary lamellae grow out from the nucleus, there is a tendency for them to become splayed and branched, which is responsible for the ultimately near-spherical nature of these structures. Near the periphery of the spherulite the splaying results in very appreciable interlamellar spacings, which are typically on the order of thousands of angstroms. Secondary crystallization, which presumably occurs via lamellar thickening, would maintain the distribution of crystallinity similar to that of the template determined by the primary lamellae.

The crystallinity exhibits dual-population melting behavior between 180 and 230 °C. Typical DSC calorigrams of the semicrystalline matrices before and after the diffusion experiments are presented as Figure 2. Integration over both endotherms provides a nominal 52 wt % overall degree of crystallinity of $\Delta H_{fusion} = 9.0$ kJ/mol.[11] The two melting peaks are characteristic of polymers in which a population of high melting, highly ordered crystallites is surrounded within another population of less ordered, volume-filling crystallites formed later in the crystallization. This was confirmed by direct visualization by video microscopy of the matrix melting during slow heating. At a temperature of 209 °C, which corresponds to the position of the first DSC melting peak, a free-flowing melt phase was observed to form. Once the temperature had reached 212 °C, which is at the midpoint between the two melting peaks, the spherulites form an undecorated, impinging framework within the liquid melt. The overall superstructure of the spherulites persists to 218 °C, the position of the second melting peak, where they begin to melt. The last visible evidence of crystallinity at 400× magnification disappears at 223 °C.

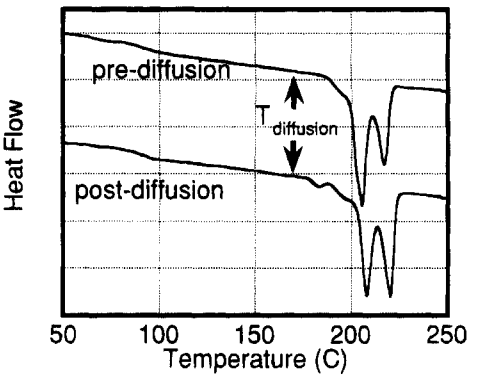

Figure 2. Differential scanning calorigrams of the pre- and postdiffusion iPS matrices. The temperature of the diffusion experiments (170 °C) is 13 °C lower than the onset crystallization temperature. Although no gross morphological change in the matrix occurs during the experiment, some annealing does occur as evidenced by the small melting endotherm at 186 °C and the increased melting temperature of the two dominant crystallite populations.

Table 3. Summary of SAXS Data and Computed Lamellar Variables as a Function of Temperature: SAXS Peak Position (q_{max}), Peak Area (Q) Long Period Spacing (L), Linear Degree of Crystallinity (x_{CL}), Lamellar Thickness (l_C), and Average Amorphous Pocket Size (d_a)

T (°C)	q_{max} (nm^{-1})	Q (au)	L(Å)[a]	x_{CL} (%)[a]	l_C (Å)[b]	$_a$ (Å)[c]
31	0.441	0.0939	139	69.2	96	265
111	0.436	0.1535	140	69.1	97	270
144	0.430	0.1952	140	68.1	95	250
162	0.427	0.2072	140	67.0	94	240
173	0.418	0.2179	144	67.8	98	260

[a] Calculated by correlation function $\gamma(r)$. [b] $l_C = x_{CL}L$. [c] $\phi_C = n\, l_C/(d_a + nL)$, $n = 5$, $\phi_C = 0.50$.

The matrix is not perfectly static over the course of a diffusion experiment. This is seen in the appearance of a third population of crystallites with a peak melting at 186 °C in the postdiffusion DSC of Figure 2. The slow growth of crystallites which melt 10–20 °C above the annealing temperature is common in polymer systems. Augmented crystallization of the parent populations also occurs, with peak melting temperatures increasing by 3–5 °C. The lower melting population is ca. 63% of the total crystallinity before diffusion and ca. 59% after diffusion. We note these reflect very minute changes to the overall degree of crystallinity and morphology. Since the secondary crystallization reflects perfection of order on a local scale, this process occurs much more rapidly than the macromolecular center-of-mass transport into the matrix.

Two features are seen in the SAXS data. First, the peak scattering position, q_{max}, decreases with increasing temperature from which we infer the scattering domains increase in average size. Second, the area of the intensity spectrum, Q, as a function of temperature has a maximum at 173 °C, where we would hence surmise the highest degree of crystallinity. Similar features have been seen in other semicrystalline polymers such as PEEK during melting by time-resolved SAXS measurements.[6] The results of the SAXS analyses are provided in Table 3.

It has long been appreciated that spherulite structure is heterogeneous and complex and that any tractable morphological model necessarily incorporates enormous simplifications. Despite this caveat, such models can provide insight into the important features which govern transport within the spherulite. We adopt the correlation function approach of Santa Cruz *et al.*[7] in

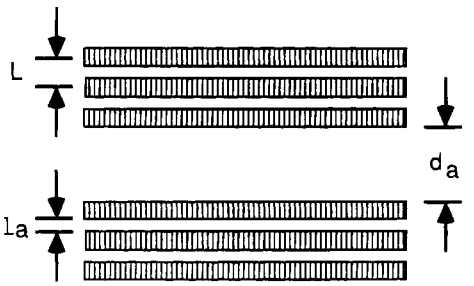

Figure 3. Schematic representation of a two-phase model showing bundles of lamellae of long period L and spacing l_a separated by a large amorphous region of width d_a. The lamellar thickness is l_C.

the analysis of SAXS data, which invokes the morphological model illustrated in Figure 3. In this hierarchical model, a spherulite is comprised of many bundles of lamellae. The bundles are further segregated by an intervening amorphous phase, which we refer to as amorphous pockets. It is important to recognize that the SAXS experiment probes length scales between the magnitudes of 1−1000 Å, only a significant fraction of the distribution of interlamellar spacings. Hence, the characteristic dimensions extracted from the SAXS data using the aforementioned model are averages taken over these limited length scales. The average dimensions derived from this analysis are also presented in Table 3. The value of the long period, L, increases slightly with temperature until 173 °C and then increases to 13%. These values agree extremely well with SAXS and TEM results on iPS in the literature.[12] The linear degree of crystallinity, x_{CL}, decreases consistently with increasing temperature. As a result, the lamellar thickness, the product of L and x_{CL}, first decreases and then increases with increasing temperature. Once the temperature reaches 196 °C, it is apparent that partial melting occurs, which results in an increase of L and decrease of both x_{CL} and Q. The value of l_C increases, which may be due to the thicker or thickened residual lamellae. SAXS measurements at 210 °C show no scattering signals.

The SAXS results at 173 °C are the most relevant to the experimental conditions presented herein. These suggest that the isotactic matrix consists of crystalline obstacles 720 Å wide (i.e., 5 times the long period), separated by amorphous pockets 260 Å in width. The characteristic dimension, d_A, of the amorphous pockets does not change remarkably with temperature below the melting point after sufficient annealing. We believe that these pockets are the primary arteries for penetrant transport, as we discuss in more detail below. However, these SAXS interpretations represent only a coarse average of the heterogeneous structure since the SAXS measurements are incapable of determining structural correlations larger than ca. 0.1 μm. We have already noted that interlamellar spacings can be much larger than this at the periphery of a spherulite. TEM studies[8-10] clearly show severe heterogeneity in the distribution of amorphous volume within the spherulites. The actual spherulite will contain a large volume of material inaccessible to penetrant macromolecules in the center, and large volumes of accessible material at the periphery.

This structural heterogeneity renders it difficult to investigate the precise details regarding transport, since it is unlikely that transport occurs with similar ease everywhere in the spherulite. Transport will be limited to those regions in which the lameller structure has defined channels of a dimension adequate to accommodate a penetrant macromolecule. Furthermore, the nature of the spherulite growth may also mean that some of the channels become dead ends as the interlamellar spacing diminishes near the nucleus. Hence the typical penetrant path must be tortuous and the cross-sectional passage area must change dramatiaclly along the path.

Diffusion in Atactic Melts. In our initial measurements of aPS-D diffusion into aPS melts,[2] we found that the tracer diffusion coefficients inferred from the ATR technique were close to, but systematically smaller than, those reported previously from ion-beam experiments.[13,14] We have generated further data so that we can both explore further the discrepancy with literature data on melts and compare polymer transport into melt and semicrystalline matrices based on methodologically consistent data.

First, we juxtapose our ATR-FTIR technique with other methods. Our experimental conditions measure the tracer diffusion coefficient since the initial thickness of the penetrant on the ATR crystal is much thinner than the penetration depth of the evanescent IR beam.[2] Advantages of the ATR technique include the collection of data with high signal-to-noise ratios with even very thin films and the ability to acquire numerous data during the diffusion experiment, which is typically run between 10^4 and 10^5 s. This longer experimental time frame also diminishes the influence of experimental artifacts such as the orientation of the films from the solution-casting process,[15] inclusion of residual solvent,[16] and the finite time required for molecular scale interface formation between the diffusion couple.[17] Polymer interdiffusion rates can be very sensitive to variations in sample preparation. Specifically, the annealing of solution-cast polymer films is critical for minimizing artifacts cause by the dynamics of the coating process, since in the process of spin and dip coating the rate of evaporation of solvent can be much faster than the rate of interchain reentanglement. This results in a glassy film in which chains are not entangled to the same degree as if the glass was obtained by quenching an equilibrium melt.[15,16] In addition, annealing individual layers of the diffusion couple separately cannot create a bulk entanglement concentration near the interface until the actual diffusion experiment. As a consequence, macromolecular interdiffusion rates are enhanced until the bulk entanglement concentration is established at the diffusion couple interface. We have found these effects particularly prevalent in our studies using the highest molecular weight ($N = 5000$). As an illustration, data reported in our previous study[2] are replotted here in semilogarithmic fashion in Figure 4. Figure 4 illustrates the uptake behavior for $N = 5000$ aPS-D dissolving into a solution-cast film of $N = 19\,710$ of aPS. The early time (<10 h) data alone would yield a diffusion coefficient greater by a factor of 3 than that fit from the course of the entire experiment. Accurate diffusion data of high polymers are more reliably obtained by obtaining diffusion data over the entire time scale of interdiffusion.

Figure 5 illustrates the dependences of penetrant diffusivity on molecular weight in two independent series of experiments performed at 170 °C. All diffusivities were obtained by fitting the ATR uptake as a function of time using eq 1 allowing only the diffusivity value as a degree of freedom. Uncertainties in the

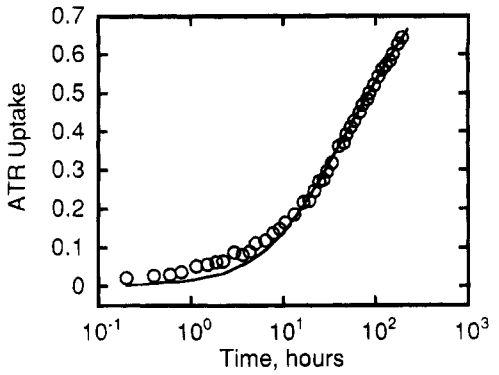

Figure 4. Diffusion data for an atactic, $N = 5000$ aPS-D penetrant in an atactic, $N = 19\,710$ PS matrix at 170 °C.

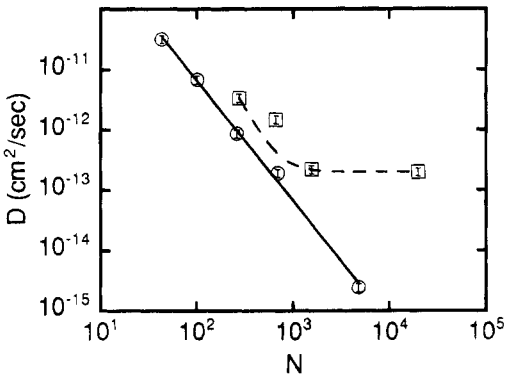

Figure 5. Polystyrene tracer diffusivities at 170 °C in polystyrene. The open circles indicate the penetrant diffusivity as a function of the penetrant molecular weight, each for the same matrix for which $N = 19\,710$. The solid line fit is expressed in eq 3. The open squares indicate the effect of increasing the matrix molecular size for the same penetrant $N = 1040$. The dashed line fit is expressed in eq 5.

diffusivities are less than 10%. The numerical values are provided in Table 2.

The data represented by open circles in Figure 5 illustrate the effect of increasing the penetrant degree of polymerization, N_p, holding constant the matrix degree of polymerization, $N_m = 19\,710$, in the series of experiments. These data reflect the limiting diffusivities of penetrants whose lengths are greater than the critical length for entanglement, N_e, in a very high polymer matrix. The data are well correlated by

$$D = \frac{5.28 \times 10^{-8}\ (\mathrm{cm^2/s})}{N_p^{1.92}} \qquad (3)$$

as illustrated by the solid line fit in Figure 5. The power law dependence on molecular weight being near −2 agrees well with that predicted by reptation theory.[18] When the right-hand side denominator is expressed in terms of molecular weight, the resulting numerator, D_0, is 5.71×10^{-3} cm²/s. Our value of D_0 agrees quite favorably with theoretical predictions of 4×10^{-3} cm²/s[19] and other experimental determinations of 8×10^{-3} cm²/s[20] at 170 °C. Our activation energy values provided in Table 4 also are in fair agreement with the literature values reviewed by Tirrell.[21] Von Meerwall *et al.*[22] also observed that the diffusivity activation energy increases with molecular weight and correlated this effect well using free volume theory. We believe that chain ends are far less constrained than the middle chain segments, and this condition may be viewed also as an increase in the local unoccupied volume within which segmental motions would be enhanced. This would result in a smaller apparent activation energy for lower molecular weight species.

Table 4. Activation Energy (E_A) for aPS-D Tracer Diffusion Coefficients in aPS Matrices for Which $N = 19\,710$

T_{avg} (°C)	$N_{penetrant}$	E_A (kJ/mol)	E_A/RT_{avg}
150	45	42.7 ± 13.0	12.4
150	1 040	107.1 ± 8.4	30.5

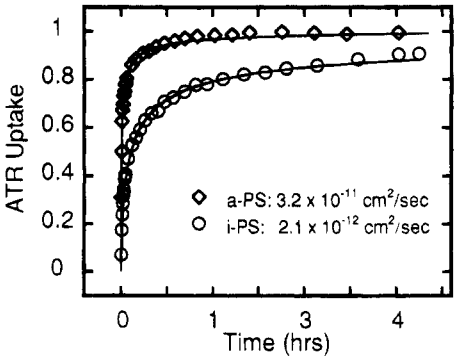

Figure 6. Comparison of the diffusion of an atactic, $N = 270$ aPS-D penetrant into matrices of atactic, $N = 19\,710$ aPS (diamonds) and semicrystalline, $N = 5910$ iPS at 170 °C. The Fickian uptake model fits well both data sets.

The data represented by open boxes in Figure 5 indicate the effect of various matrix molecular sizes for the same penetrant $N_p = 1040$. The plateau near $N_m = 1000$ indicates that the effective entanglement length here is essentially the same size as the penetrant. These data are correlated favorably assuming that reptation and constraint release mechanisms occur independently.[23] For a polymer tracer diffusion coefficient, D_t, Green *et al.*[9] correlate their ion-beam measurements of polystyrene-*d*/polystyrene interdiffusion using

$$D_t = \frac{D_0}{N_p^2} + \frac{\alpha_{CR} D_0 N_e^2}{N_p N_m^3} \qquad (4)$$

where α_{CR} is a constant which depends on the number of constraints per entanglement.[23] The dashed line fit in Figure 5 pertains to

$$D = 2.0 \times 10^{-13} + \frac{(6.8 \pm 1.1) \times 10^{-5}}{N_m^3}\ (\mathrm{cm^2/s}) \qquad (5)$$

Through somewhat limited in number, these data also indicate qualitatively favorable agreement, comparable to that obtained previously.[13]

aPS-D Transport in Semicrystalline iPS. It is of interest to contrast the imbibition phenomenology and kinetics of deuterated penetrants in amorphous and semicrystalline matrices. Figure 6 illustrates one example for the penetrant with a degree of polymerization $N = 45$. The Fickian mutual diffusion model in eq 1 can describe the transport kinetics of both experiments. Transport into the semicrystalline matrix is characterized by a diffusion coefficient of 2.1×10^{-12} cm²/s, which is over 1 order of magnitude lower than the value of 3.2×10^{-11} cm²/s for the same penetrant in an amorphous, high molecular weight matrix. For imbibition of the penetrant $N = 5000$, the contrast between the amorphous and semicrystalline matrices is even more striking; see Figure 7. Not only is the imbibition into

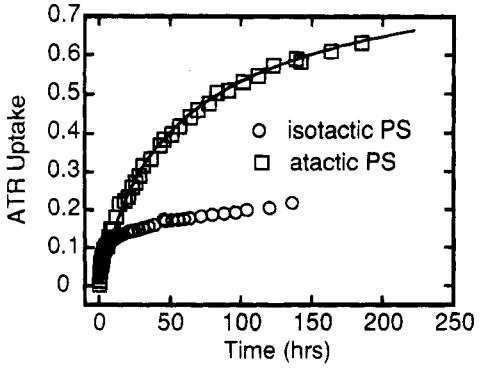

Figure 7. Comparison of the diffusion of an atactic, $N = 5000$ PS-D penetrant in matrices of atactic, $N = 19\,710$ PS (squares) and semicrystalline, $N = 5910$ iPS (circles) at 170 °C. It is impossible to obtain fits of the uptake into the isotactic matrix using a Fickian model.

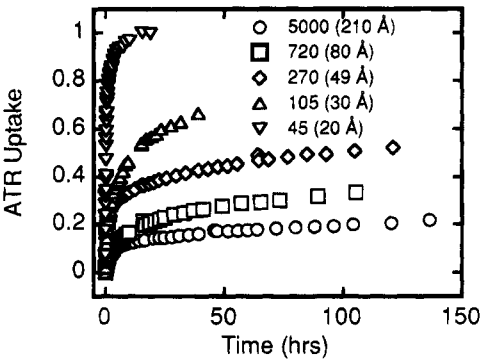

Figure 8. Comparison of the transport kinetics of penetrants of various degrees of polymerization into $N = 5900$ isotactic polystyrene at $T = 170$ °C. The transport rate diminishes very rapidly as the chain radius of gyration (parentheses) becomes comparable to the average size of the amorphous pockets within the semicrystalline matrix.

the isotactic matrix severely limited, but the Fickian model can only fit the imbibition data into the amorphous, atactic matrix. For the imbibition into the isotactic matrix, the short-time uptake kinetics are Fickian with a restricted level of imbibition and the long-time uptake proceeds with sub-Fickian kinetics. Similar behavior was also reported previously in the PEI/PEKK system.[1] Figure 8 illustrates the transport kinetics of several perdeuterated penetrants with degrees of polymerization ranging from 45 to 5000 into identical semicrystalline matrices. The imbibition rate into the semicrystalline matrix diminishes rapidly as the chain length of the penetrant increases. Imbibition kinetics of all but the smallest penetrant, $N = 45$, are non-Fickian.

We next consider transport of the $N = 45$ penetrant into semicrystalline matrices at various temperatures below the crystalline melting range. Figure 9 illustrates that fits of the early time data using the Fickian mutual diffusion model can be obtained over early time data from the experiments performed at 150 and 170 °C. In contrast, the kinetics of the 130 °C experiment are non-Fickian. The kinetics at 130 °C being slower than Fickian are qualitatively similar to the higher molecular weight penetrant imbibition kinetics at 170 °C. If the experimental temperature is subsequently raised from 130 to 170 °C, sorption of the penetrant proceeds rapidly and completely. The occurrence of a transition between Fickian and non-Fickian phenomenology with both temperature and penetrant molecular weight provides an essential characterization for the origin of the non-

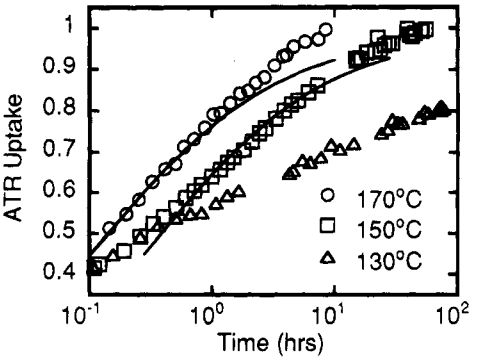

Figure 9. Temperature dependence of the transport for an $N = 45$ penetrant into iPS, with experiemental data (symbols) illustrated with Fickian fits (lines). It is impossible to obtain reasonable fits for the lowest temperature (130 °C) experiment.

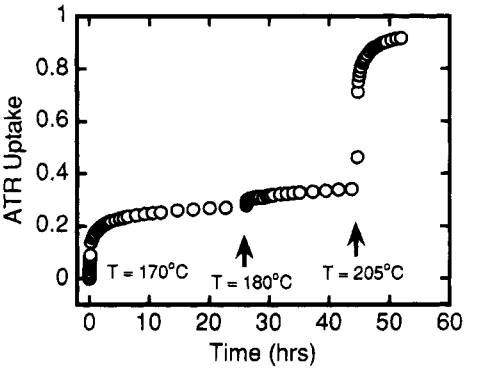

Figure 10. Influence of crystalline melting on transport for an $N = 270$ penetrant into iPS. At 170 and 180 °C, with little or no melting, transport proceeds in a slow, monotonic fashion. At 205 °C, corresponding to the first melting peak of the matrix (see DSC of Figure 2), the matrix forms a free liquid phase and allows the penetrant and molten material to diffuse mutually.

Fickian kinetics which we will propose in the Discussion section.

Transport and Crystalline Melting. It is informative to observe how the transport kinetics change as the experimental temperature is increased into the melting range of the matrix. This was investigated in an experiment using the $N = 270$ penetrant and a ZnS ATR crystal, which has a wider spectral band-pass than silicon over the IR wavelengths of interest. Figure 10 presents the normalized uptake monitored for the imbibition of the penetrant as the temperature is increased incrementally; the melting behavior of this matrix is displayed in Figure 2. At temperatures of 170 and 180 °C, below the crystalline melting range, the normalized uptake proceeds with the non-Fickian, two time scale kinetics we have described previously. Once the temperature is increased to 205 °C, to the first melting peak, the imbibition of penetrant proceeds quickly to completion with Fickian kinetics and a diffusion coefficient estimated to be 2.0×10^{-12} cm^2/s. This can be understood in light of the melting behavior observed optically, which indicated that a molten phase forms near this temperature, thus allowing the penetrant and partially melted matrix to diffuse mutually.

Discussion

Empirically, we observed non-Fickian transport kinetics during the imbibition of macromolecular penetrants into semicrystalline polymers at low temperatures and high penetrant molecular weights. There are two

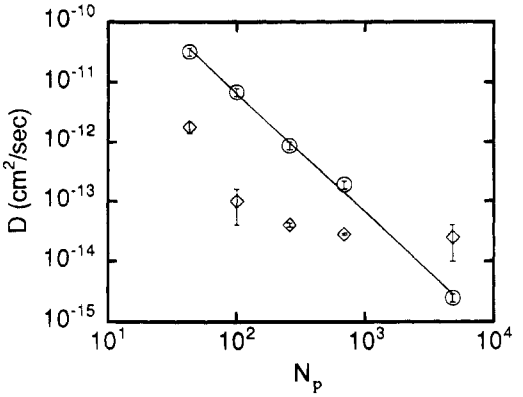

Figure 11. Comparison of the diffusion coefficients for PS-D penetrants of chain length N in amorphous aPS matrices (circles) and the coefficients obtained from the *early time* penetration of semicrystalline iPS (diamonds). The plateau in the semicrystalline behavior may indicate that transport in this regime is governed by the countercurrent flux of uncrystallized iPS.

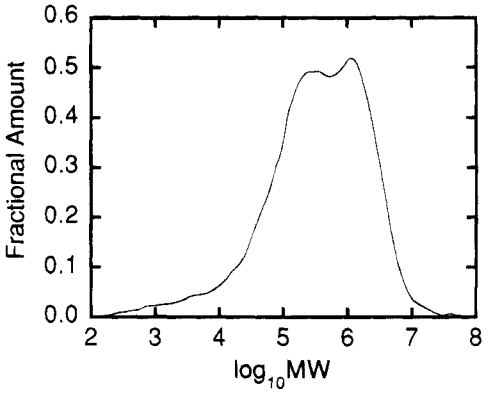

Figure 12. Our independent measurement of the $N_m = 19\,710$ isotactic polystyrene matrix molecular weight distribution using GPC in trichlorobenzene.

apparent time regimes of non-Fickian kinetics. The first regime of imbibition kinetics occurs at early times where the uptake can be described by Fickian mutual diffusion kinetics. Later, there is a decrease in the imbibition rate and the rates of continued imbibition can no longer be described using a simple Fickian model. The transition and later regime kinetics depend strongly on temperature, the penetrant polymer length, and matrix polymer morphology. We attempt to interpret this phenomenology in the following discussion.

Some very interesting physics are revealed in the early time imbibition in the semicrystalline matrices. We consider in more detail aPS-D imbibition into the $N_m = 5900$ semicrystalline iPS at 170 °C. Early time, Fickian mutual diffusivities can be obtained by truncating the uptake data after the observed imbibition rate discontinuity and fitting the diffusivity in eq 1 to the remaining early data. The fits are comparable to those illustrated in Figure 9, which also demonstrates that only the early time data can be described by Fickian kinetics. The open diamonds in Figure 11 depict these early time diffusivities as a function of penetrant degree of polymerization. The error bars each indicate the range of uncertainty in the fitted values as determined from statistical error propagation; the method is described in our previous work.[2] The surprising result is the apparent plateau in the diffusivity at N_p values above ca. 10^3. For comparison, the open circles in Figure 11 represent the tracer diffusivities of the same penetrants in amorphous, $N_m = 5900$ matrices at 170 °C. The solid line fit represents eq 3. There is an intersection between these two data sets at approximately $N_p = 1600$ which occurs within the plateau of the early time diffusivity curve. This suggests that the early time penetration kinetics into this semicrystalline matrix are influenced by countercurrent diffusion of amorphous, isotactic polymer up to length ca. $N = 1600$, in addition to the dendritic obstacles within the semicrystalline matrix.

This mechanism for the early time regime is consistent with the matrix composition and morphology. Gel permeation chromatography of the iPS matrix (see Figure 12) indicates that approximately 20% of the matrix is comprised of chain lengths below $N = 10^3$. Hence if this low molecular weight fraction is amorphous, it would comprise an appreciable fraction of material which would be capable of diffusing much more rapidly than the longer length penetrant and crystalline matrix chains. The presence of a lower molecular weight, faster moving species dominates the mutual diffusion flux as outlined by Kramer.[24] In addition, it is well established in the polymer crystallization literature that low molecular weight materials are preferentially segregated from the crystalline phase during the formation of spherulitic morphologies.[25,26] More precisely, the short chains tend to segregate from the longest, most readily crystallized chains and create the amorphous pockets of the matrix. In this state, the short chains would be readily available to diffuse mutually with a contacting penetrant phase. During this early time regime, Fickian diffusion kinetics are fully expected. We will consider the effects of dendritic crystallites on the interdiffusion rate after considering possible mechanisms for the non-Fickian interdiffusion observed after the early time kinetics regime.

Currently, there are few known mechanisms which can account for non-Fickian macromolecular transport kinetics. The results of the previous section strongly suggest that only minute changes in the semicrystalline morphology occur during imbibition of aPS-D. Specifically, the IR spectra measured during interdiffusion remained unchanged, and only minute changes were noted via calorimetry and X-ray scattering after the entire imbibition experiments. Hence we cannot attribute the non-Fickian interdiffusion phenomenology to bulk, structural changes within the matrix. Next, we consider the possibility of variable mutual diffusivity. Although the PEI penetrant molecular weight distribution in our previous study[1] is polydisperse, the aPS-D penetrants used in this study are highly monodisperse. Hence we cannot attribute non-Fickian kinetics to penetrant size polydispersity. Given the strong chemical similarity between the aPS-D penetrants and iPS matrices, enthalpic driving forces are minute. Hence interdiffusion is motivated primarily by an entropic gradient driving force and we do not expect appreciably concentration-dependent mobilities. The local mobility might be considerably different through interdendrite channels than through the boundaries which define individual spherulite domains. However, even the existence of very different mobilities between the two conducting regions within the matrix is insufficient to explain the onset of anomalous kinetics. In this case Fickian kinetics would still be expected. A spectrum of mobilities may exist spatially given polydispersity in the size and tortuosity of the pathways provided by chaotically organized, amorphous pockets in iPS matrices. From optical microscopy it is apparent that the average

spherulite diameter and the matrix film thicknesses are comparable; therefore the penetrant mobility will be controlled by the morphological details within a single spherulite layer. Hence we must consider that the existence of distinct kinetic regimes can be a signature of transport within the chaotic, heterogeneous semicrystalline morphology itself as suggested previously.[1]

Non-Fickian diffusion has been previously discovered in heterogeneous media due to percolation and configurational effects. First, we review briefly the signature of transport into a medium in which conducting regions just attain a percolation threshold. The effective medium theory of Sahimi *et al.*[27] predicts only three kinds of behavior for transport in disordered media where only a fraction of the pathways transmit a random walking diffusant. The analysis considers a single-bond effective medium approximation to the bond percolation threshold, p_c. The diffusant's mean-squared displacement remains localized for porosities below p_c, fractal with transport slower than Fickian for porosities near p_c, and classical Fickian diffusion for porosities above p_c. Ottino and Shah[28] have simulated transient sorption in these three percolation regimes which illustrate similar phenomenology. Classical sorption occurs for porosities above p_c. In media with porosities below p_c, there is pseudoclassical sorption to a diminished level of imbibition which depends on the total porosity. At this time no further sorption occurs; i.e., a second kinetic regime does not occur. In the iPS matrices, the total volume fraction of material found in the amorphous phase is approximately 0.5. This suggests that amorphous phase percolates the entire thickness of the matrix. Hence the onset of the non-Fickian sorption regime might not be most accurately identified as a signature of transport near the critical percolation threshold.

Next, we consider the effects of randomly distributed, entropic barriers on macromolecular transport. Muthukumar and Baumgartner[29-32] provide simulations of chains undergoing Brownian motion while ensconced between both regularly spaced and randomly distributed, impenetrable obstacles. In random media there are three time regimes of the center-of-mass mean-squared displacement. At short times there are Fickian kinetics due to the unhindered displacement over distances smaller than the average separation between obstacles. At intermediate times the chain explores bottlenecks and narrow channels between obstacles over time scales comparable to the correlation time of the chain's radius of gyration. Anomalous, sub-Fickian diffusion kinetics result as chain configurational motion is retarded. The termination time which characterizes the crossover of the transport from anomalous to Fickian diffusion occurs as the chain has explored bottlenecks to several obstacles. Muthukumar and Baumgartner[30] suggest that long-time diffusivity can be described by the chain's partitioning between the bottlenecks and open pockets. From relatively simple arguments, the ratio of the long-time tracer diffusivity, D, relative to the chain's diffusivity, D_0, in the absence of obstacles scales according to

$$\ln\left(\frac{D}{D_0}\right) = -N\left\{f\left(\frac{1}{C}\right)^{1/\nu} + \left(\frac{1-f}{z} - 1\right)\left(\frac{1}{C_1}\right)^{1/\nu}\right\} \quad (6)$$

where f is the fraction of monomers inside a bottleneck, C is the average bottleneck size, C_1 is the average pocket size, z is the average number of open domains per bottleneck, and ν is the Flory exponent expressing the dependence of the diffusing chain's radius of gyration on the degree of polymerization; i.e., $R_G \sim N^{\nu}$. In the limit where chains are much longer than the bottlenecks, $f \sim N^{-1}$. Anomalous diffusion did not appear in media with periodically distributed obstacles. This suggests that matrix disorder plays an important role in chain dynamics.

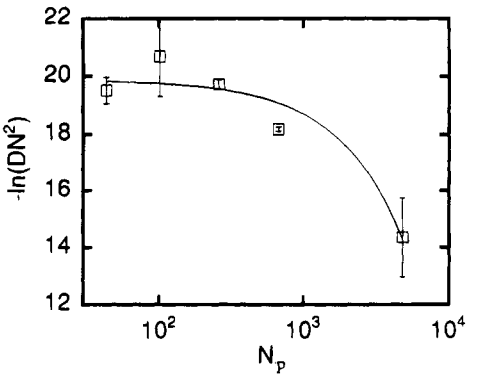

Figure 13. Early time diffusion coefficients of PS-D penetrants in iPS matrix N_m = 19 710 as a function of penetrant degree of polymerization (open squares) and fit of eq 7 (solid line).

The effective diffusivities, D_{eff}, in Figure 11 which were extracted from the early time regime differ from the diffusivity, D, in eq 6 in two respects. First, D_{eff} is an effective mutual diffusion coefficient, since there is counter current flow between the penetrant and amorphous matrix chains. In contrast, D reflects the steady-state mean-squared displacement of a single chain ensconced in a disordered medium. Second, the observation of aPS-D near the ATR crystal surface measures both mutual diffusion in the melt layer near the surface and the kinetics of aPS-D exploring crystalline obstacles through the matrix. Even at early times, however, the aPS-D chains closest to the semicrystalline matrix begin passage into the spherulites. Further, we expect this process to be rate limiting. Hence, D_{eff} primarily reflects the mobility of penetrant chains in the disordered, semicrystalline medium. In order to apply eq 6, we recognize that the reference diffusivity D_0 should follow an inverse-squared dependence on molecular weight, similar to eq 3. Hence the relationship between D_{eff} and N_p should follow

$$-\ln(D_{eff}N_p^2) = AN_p + B \quad (7)$$

where A and B are constants which depend on only the matrix morphology for a given polymer whose length is much longer than the bottlenecks. The left-hand side of eq 7 is plotted as a function of N_p in Figure 13. Error bars are again determined from propagated uncertainties. The solid line indicates the best fit to these data by eq 7 optimizing constants A and B. Our set of data points is somewhat limited in quantity but so far indicates favorable agreement nonetheless with $A = 1.17 \times 10^{-3}$ and $B = 19.9$.

If the aforementioned model is appropriate in the analysis of the early time regime, then we would expect that crystalline obstacles would at most hinder chain transport by increasing the penetrant path tortuosity and cross-sectional passage area but not affect appreciably the elementary, segmental motions which ultimately provide center-of-mass motion. We believe the early time regime is dominated by interdiffusion via amorphous pathways. It is then important to consider the calculated diffusion coefficient activation energy. For

the $N = 5900$ penetrant in semicrystalline and amorphous high molecular weight matrices, the activation energies are 19 ± 3 and 22 ± 3 kcal/mol, respectively, near 170 °C. This suggests that the microscopic details of chain motion are similar both during interdiffusion between amorphous melts and during the early regime of imbibition into the semicrystalline morphologies.

Acknowledgment. We gratefully acknowledge Brian Cox for his assistance in preparing and utilizing the samples for diffusion measurements.

References and Notes

(1) Lustig, S. R.; Van Alsten, J. G.; Hsiao, B. *Macromolecules* **1993**, *26*, 3885.
(2) Van Alsten, J. G.; Lustig, S. R. *Macromolecules* **1992**, *25*, 5069.
(3) Harrick, N. J. *Internal Reflection Spectroscopy*; Wiley: New York, 1967.
(4) Salzberg, C. D. *J. Opt. Soc. Am.* **1957**, *47*, 244.
(5) Chu, B.; Wu, D. Q.; Howard, R. *Rev. Sci. Instrum.* **1989**, *60*, 3224.
(6) Hsiao, B. S.; Gardner, K. H.; Wu, D. Q.; Chu, B. *Polymer* **1993**, *34*, 3986.
(7) Santa Cruz, C.; Stribeck, N.; Zachmann, H. G.; Balta Calleja, F. J. *Macromolecules* **1991**, *24*, 5980.
(8) Basset, D. C. *CRC Crit. Rev. Solid State Mater. Sci.* **1984**, *12*, 97.
(9) Vaughan, A. S.; Bassett, D. C. *Polymer* **1988**, *29*, 1397.
(10) Bassett, D. C.; Vaughan, A. S. *Polymer* **1985**, *26*, 717.
(11) Brandrup, J.; Immergut, E. H. *Polymer Handbook*, 3rd ed.; Wiley-Interscience: New York, 1989.
(12) Yeh, G. S. Y.; Lambert, S. L. *J. Appl. Phys.* **1971**, *42*, 12.
(13) Green, P. F.; Mills, P. J.; Palmstrom, J.; Mayer, J. W.; Kramer, E. J. *Phys. Rev. Lett.* **1984**, *53*, 2145.
(14) Green, P. F.; Kramer, E. J. *Macromolecules* **1986**, *19*, 1108.
(15) Sauer, B. B.; Walsh, D. J. *Polym. Mater. Sci. Eng. Preprints.* **1993**, *69*, 185.
(16) Fernandez, M. L.; Higgins, J. S.; Penfold, J.; Shackleton, C. S. *Polym. Commun.* **1990**, *31*, 124.
(17) Kim, Y. H.; Wool, R. P. *Macromolecules* **1983**, *16*, 1115.
(18) de Gennes, P.-G. *Scaling Concepts in Polymer Physics*; Cornell University Press: Ithaca, NY, 1979.
(19) Graessley, W. W. *J. Polym. Sci., Polym. Phys. Ed.* **1980**, *18*, 27.
(20) Mills, P. J.; Green, P. F.; Palmstrom, C. J.; Mayer, J. W.; Kramer, E. J. *Appl. Phys. Lett.* **1984**, *45*, 957.
(21) Tirrell, M. *Rubber Chem. Technol.* **1984**, *57*, 523.
(22) von Meerwall, E.; Grigsby, J.; Tomich, D.; van Antwerp, R. *J. Polym. Sci., Polym. Phys. Ed.* **1982**, *20*, 1037.
(23) Graessley, W. W. *Adv. Polym. Sci.* **1982**, *47*, 67.
(24) Kramer, E. J.; Green, P.; Palmstroem, C. J. *Polymer* **1984**, *25*, 473.
(25) Keith, H. D.; Padden, F. J., Jr. *J. Appl. Phys.* **1964**, *35*, 1270.
(26) Keith, H. D.; Padden, F. J., Jr. *J. Appl. Phys.* **1964**, *35*, 1286.
(27) Sahimi, M.; Hughes, B. D.; Scriven, B. D.; Davis, H. T. *J. Chem. Phys.* **1983**, *78*, 6849.
(28) Ottino, J. M.; Shah, N. *Polym. Eng. Sci.* **1984**, *24*, 153.
(29) Baumgartner, A.; Muthukumar, M. *J. Chem. Phys.* **1987**, *87*, 3082.
(30) Muthukumar, M.; Baumgartner, A. *Macromolecules* **1989**, *22*, 1937.
(31) Muthukumar, M.; Baumgartner, A. *Macromolecules* **1989**, *22*, 1941.
(32) Baumgartner, A. In *Springer Series in Chemical Physics*; Tanaka, F., Doi, M., Ohta, T., Eds.; Springer-Verlag: Berlin, 1989; Vol. 51.

MA9461097